

Dynamics of cluster formation in driven dipolar colloids dispersed on a monolayer

Sebastian Jäger, Holger Stark, and Sabine H. L. Klapp

Institute of Theoretical Physics, Technical University Berlin,
Hardenbergstr. 36, 10623 Berlin, Germany

E-mail: jaeger@itp.tu-berlin.de

Abstract. We report computer simulation results on the cluster formation of dipolar colloidal particles driven by a rotating external field in a quasi-two-dimensional setup. We focus on the interplay between permanent dipolar and hydrodynamic interactions and its influence on the dynamic behavior of the particles. This includes their individual as well as their collective motion. To investigate these characteristics, we employ Brownian dynamics simulations of a finite system with and without hydrodynamic interactions. Our results indicate that particularly the translation-rotation coupling from the hydrodynamic interactions has a profound impact on the clustering behavior.

1. Introduction

Systems of colloidal particles can organize into a wide variety of different structures, both under equilibrium conditions (“self-assembly”) and in nonequilibrium. Prime examples of nonequilibrium structure formation are lane formation of charged colloids [1, 2], shear banding of rod-like particles [3], the coiling up of chains of magnetic colloids [4], metachronal waves in driven colloids [5], and the formation of colloidal caterpillars [6].

Indeed, magnetic particles form a particular subset of colloidal systems, since they can be easily manipulated by external magnetic fields. The interplay of particle-field interactions and the anisotropic (dipole-dipole) magnetic interactions between the particles then leads to a wide variety of structures such as chains [7, 8, 9], layers [9, 8, 10, 11, 12], and intricate honeycomb-like structures [13, 14, 15].

In this study we want to focus on the pattern formation of dipolar particles that are driven by a rotating field. In three-dimensional systems dipolar particles exposed to such a field tend to form layers (biaxial field) [16, 11] or membrane-like structures (triaxial field) [13, 14]. In a two-dimensional geometry, in which the external field rotates in the plane of the particles, the dipoles tend to agglomerate into clusters. This phenomenon has been observed experimentally [17, 18] as well as in computer simulations that were performed by two of the authors of this study [19]. Clustering does not only occur for particles carrying a permanent dipole moment, but also for particles with an induced dipole moment [20, 21, 22].

At suitable fields strengths and frequencies, the (permanently) dipolar particles perform a synchronous rotation with the field. This motion gives rise to an attractive, long-range particle interaction ($\propto -1/r^3$), which induces a first-order phase transition between a dilute and a denser phase (in an infinitely extended system). The observed cluster formation then corresponds to spinodal decomposition inside of the coexistence region [19].

It has been shown that hydrodynamic interactions play a crucial role in numerous colloidal systems [23, 24, 25, 26]. The influence of hydrodynamic interactions on the clustering phenomenon was, however, only shortly touched upon in [19]. Here, in this study, we want to look into the effects that an implicit solvent has on the cluster formation and the dynamic behavior of the particles in more detail.

The main tool we use are Brownian dynamics computer simulations with and without hydrodynamic interactions. The particles are modeled by a quasi-two-dimensional system of soft spheres with permanent dipole moments. This means that the dipoles can rotate freely in all the spatial directions, while the translational motion is restricted to a two-dimensional plane. In our hydrodynamic simulations, we not only account for the translational hydrodynamic couplings, but for all the couplings between the translational and rotational motions of the particles. To understand the influence of these different couplings is one of the goals of this study. Contrary to [19], we here consider a finite system size, i.e., we do not employ periodic boundary conditions.

This paper is organized as follows: After introducing the model and the simulation techniques, we discuss the influence of hydrodynamic interactions on the regions of cluster formation in the field strength-frequency domain. To understand the differences stemming from the solvent interactions, we also consider the magnetization and synchronization behavior of the particles. In a next step, we investigate the dynamics of the clusters and their formation. Finally, we examine the structure of the clusters with respect to their internal order. The paper is then closed with a brief summary and conclusions.

2. Model and simulation methods

In this study, we consider a quasi-two-dimensional system of dipolar colloidal particles that are immersed in a solvent. As a model for the colloids we use a dipolar soft sphere (DSS) potential, which is comprised of a repulsive part U^{rep} and a point dipole-dipole interaction part U^{D} :

$$U^{\text{DSS}}(\mathbf{r}_{ij}, \boldsymbol{\mu}_i, \boldsymbol{\mu}_j) = U^{\text{rep}}(r_{ij}) + U^{\text{D}}(\mathbf{r}_{ij}, \boldsymbol{\mu}_i, \boldsymbol{\mu}_j) \quad (1)$$

In (1), \mathbf{r}_{ij} is the vector between the positions of the particles i and j , r_{ij} its absolute value, and $\boldsymbol{\mu}_i$ is the dipole moment of the i th particle. The dipolar and repulsive interaction potentials are given by

$$U^{\text{D}}(\mathbf{r}_{ij}, \boldsymbol{\mu}_i, \boldsymbol{\mu}_j) = -\frac{3(\mathbf{r}_{ij} \cdot \boldsymbol{\mu}_i)(\mathbf{r}_{ij} \cdot \boldsymbol{\mu}_j)}{r_{ij}^5} + \frac{\boldsymbol{\mu}_i \cdot \boldsymbol{\mu}_j}{r_{ij}^3} \quad (2)$$

and [27]

$$U^{\text{rep}}(r) = U^{\text{SS}}(r) - U^{\text{SS}}(r_c) + (r_c - r) \frac{dU^{\text{SS}}}{dr}(r_c), \quad (3)$$

respectively. Here, U^{rep} is the shifted soft sphere potential, where

$$U^{\text{SS}}(r) = 4\epsilon \left(\frac{\sigma}{r_{ij}} \right)^{12} \quad (4)$$

is the unshifted soft sphere (SS) potential for particles of diameter σ .

We investigate the system by making use of Brownian dynamics (BD) simulations with and without hydrodynamic interactions (HIs). Specifically, the positions of the particles are evolved in time via [28, 29, 30]

$$\begin{aligned} \mathbf{r}_i(t + \Delta t) = \mathbf{r}_i(t) + \frac{1}{k_B T} \sum_j \mathbf{D}_{ij}^{\text{TT}} \mathbf{F}_j \Delta t \\ + \frac{1}{k_B T} \sum_j \mathbf{D}_{ij}^{\text{TR}} \mathbf{T}_j \Delta t + \mathbf{R}_i(\mathbf{D}, \Delta t) \end{aligned} \quad (5)$$

whereas their orientations $\mathbf{e}_i = \boldsymbol{\mu}_i/\mu$ evolve according to

$$\mathbf{e}_i(t + \Delta t) = \mathbf{e}_i(t) + \left(\frac{1}{k_B T} \sum_j \mathbf{D}_{ij}^{\text{RT}} \mathbf{F}_j \Delta t + \frac{1}{k_B T} \sum_j \mathbf{D}_{ij}^{\text{R}} \mathbf{T}_j \Delta t \right) \times \mathbf{e}_i(t) + \mathbf{R}_i(\mathbf{D}, \Delta t) \times \mathbf{e}_i(t). \quad (6)$$

The forces and torques in (5) and (6) are given by

$$\mathbf{F}_i = -\nabla_{\mathbf{r}_i} \sum_{j \neq i} U^{\text{DSS}}(\mathbf{r}_{ij}, \boldsymbol{\mu}_i, \boldsymbol{\mu}_j), \quad (7)$$

$$\mathbf{T}_i = \mathbf{T}_i^{\text{DSS}} + \mathbf{T}_i^{\text{ext}}, \quad (8)$$

where

$$\mathbf{T}_i^{\text{DSS}} = -\boldsymbol{\mu}_i \times \nabla_{\boldsymbol{\mu}_i} \sum_{j \neq i} U^{\text{DSS}}(\mathbf{r}_{ij}, \boldsymbol{\mu}_i, \boldsymbol{\mu}_j), \quad (9)$$

$$\mathbf{T}_i^{\text{ext}} = \boldsymbol{\mu}_i \times \mathbf{B}^{\text{ext}}. \quad (10)$$

In (10), \mathbf{B}^{ext} denotes an external field that is homogeneous and rotates in the plane of the dipolar monolayer. Specifically,

$$\mathbf{B}^{\text{ext}}(t) = B_0(\mathbf{e}_x \cos \omega_0 t + \mathbf{e}_y \sin \omega_0 t), \quad (11)$$

where ω_0 is the frequency of the field and B_0 its strength.

In (5) and (6), $\mathbf{D}_{ij}^{\text{TT}}$, $\mathbf{D}_{ij}^{\text{TR}}$, $\mathbf{D}_{ij}^{\text{RT}}$, and $\mathbf{D}_{ij}^{\text{RR}}$ are subtensors of \mathbf{D}^{TT} , \mathbf{D}^{TR} , \mathbf{D}^{RT} , and \mathbf{D}^{RR} . The latter are subtensors of the grand diffusion tensor

$$\mathbf{D} = \begin{pmatrix} \mathbf{D}^{\text{TT}} & \mathbf{D}^{\text{TR}} \\ \mathbf{D}^{\text{RT}} & \mathbf{D}^{\text{RR}} \end{pmatrix} \quad (12)$$

and will be specified below. The random displacements in (5) and (6) behave according to

$$\langle \mathbf{R}_i \rangle = 0, \quad (13)$$

$$\langle \mathbf{R}_i(\Delta t) \mathbf{R}_j(\Delta t) \rangle = 2\mathbf{D}_{ij} \Delta t. \quad (14)$$

The actual calculation of these displacements can be done by evaluating

$$\mathbf{R} = \sqrt{2\Delta t} \mathbf{L} \cdot \boldsymbol{\xi}, \quad (15)$$

where \mathbf{R} is the vector comprised of all the \mathbf{R}_i , $\boldsymbol{\xi}$ is a vector of normally distributed random numbers, and \mathbf{L} is a lower triangular matrix which satisfies

$$\mathbf{D} = \mathbf{L} \cdot \mathbf{L}^T. \quad (16)$$

In the present study, we take the HIs into account up to third order in the inverse particle distance, which corresponds to a far field approximation. The tensors \mathbf{D}^{TT} , \mathbf{D}^{TR} , \mathbf{D}^{RT} , and \mathbf{D}^{RR} are then given by [29, 30, 26]

$$\mathbf{D}_{ii}^{\text{TT}} = \frac{k_B T}{6\pi\eta\sigma} \mathbf{I}, \quad (17)$$

$$\mathbf{D}_{ij}^{\text{TT}} = \frac{k_B T}{8\pi\eta} \frac{1}{r_{ij}} \left[(\mathbf{I} + \hat{\mathbf{r}}_{ij} \hat{\mathbf{r}}_{ij}) + \frac{2\sigma^2}{3r_{ij}^2} (\mathbf{I} - 3\hat{\mathbf{r}}_{ij} \hat{\mathbf{r}}_{ij}) \right], \quad (18)$$

$$\mathbf{D}_{ii}^{\text{RT}} = \mathbf{D}_{ii}^{\text{TR}} = 0, \quad (19)$$

$$\mathbf{D}_{ij}^{\text{TR}} = \mathbf{D}_{ji}^{\text{RT}\dagger} = \frac{k_B T}{8\pi\eta} \frac{1}{r_{ij}^2} \boldsymbol{\epsilon} \hat{\mathbf{r}}_{ij}, \quad (20)$$

$$\mathbf{D}_{ii}^{\text{RR}} = \frac{k_B T}{8\pi\eta\sigma^3} \mathbf{I}, \quad (21)$$

$$\mathbf{D}_{ij}^{\text{RR}} = \frac{k_B T}{16\pi\eta} \frac{1}{r_{ij}^3} (3\hat{\mathbf{r}}_{ij} \hat{\mathbf{r}}_{ij} - \mathbf{I}), \quad (22)$$

where η is the viscosity of the solvent and $\boldsymbol{\epsilon}$ the Levi-Civita density, which satisfies $\boldsymbol{\epsilon}_{123} = \boldsymbol{\epsilon}_{231} = \boldsymbol{\epsilon}_{312} = 1$, $\boldsymbol{\epsilon}_{321} = \boldsymbol{\epsilon}_{213} = \boldsymbol{\epsilon}_{132} = -1$, and is equal to zero for other choices of the indices. These tensors describe the different hydrodynamic couplings, i.e., the coupling between the translational motion of the particles (TT), between the translation and the rotational motion (TR) and vice versa (RT), and the coupling between the rotational motion (RR). The specific tensor given in (17) and (18), i.e., \mathbf{D}^{TT} , is the well known Rotne-Prager tensor [31].

Note that by setting to zero all the hydrodynamic coupling tensors involving different particles $i \neq j$ in (17)-(22), one arrives at the standard algorithm for BD simulations without HIs [32].

Considering the equation of motion (5), we can see that the TR coupling relates all the torques acting on the particles, i.e., their rotational motions, to all the translational motions of the particles. Physically, the TR coupling describes how the translational motion of the particles is affected by the flow fields in the solvent that are caused by the rotations of the particles. Indeed, as we will see later, the TR/RT coupling is particularly relevant for the overall dynamical behavior of the system. It is therefore instructive to briefly illustrate the implications of this coupling for a simple two-particle system (for details, see [30, 26]).

To this end, let us consider two particles that are located at a distance from each other on the x -axis in a right-handed coordinate system. Due to the TR coupling, anticlockwise rotation (following the application of a torque) of the particle at the larger value of x results in the other particle moving in the negative y -direction. By realizing that the flow fields follow the rotation of the particle, this process can be easily understood. On the other hand, an anticlockwise rotation of the particle at smaller values of x causes the other particle to move into the positive y -direction (for a sketch, see [30]).

In this study, we consider $N = 324$ particles in a simulation box that is bounded by soft walls (cf. [33]), i.e., we do not use periodic boundary conditions. Therefore, it

is not necessary to use special techniques (e.g., Ewald sums) to treat the long-range dipole-dipole interactions. The forces and torques can be calculated directly via (2).

For convenience, we make use of the following reduced units: Field strength $B_0^* = (\sigma^3/\epsilon)^{1/2}B_0$; frequencies of the field $\omega_0^* = \omega_0\sigma^2/D_0^T$, where $D_0^T = k_B T/3\pi\eta\sigma$ is the translational diffusion constant; dipole moment $\mu^* = (\epsilon\sigma^3)^{-1/2}\mu$; time $t^* = tD_0^T/\sigma^2$; temperature $T^* = k_B T/\epsilon$; position $\mathbf{r}^* = \mathbf{r}/\sigma$. In the following we specialize to systems at temperature $T^* = 1$ and of dipole moment $\mu^* = 3$. This choice corresponds to a dipolar coupling strength of $\lambda = \mu^{*2}/T^* = 9$ that is sufficiently large to enable the system to form clusters for suitable field strengths and frequencies [19]. The density of the particles in the simulation box is of no importance in the investigated systems, since the particles typically agglomerate into a single cluster.

3. Dynamics on the particle level

Applying a rotating field in the plane of a dipolar monolayer can cause the dipolar particles to agglomerate into two-dimensional clusters [19]. This agglomeration is caused by a synchronization phenomenon: At suitable field strengths and frequencies, the particles follow the field at the same phase difference resulting in an effective interparticle interaction of the form [34, 19]

$$U^{\text{ID}}(\mathbf{r}_{ij}) = -\frac{\mu^2}{2r_{ij}^3}. \quad (23)$$

Equation (23) can be arrived at by averaging the dipole-dipole potential over one rotational period of the field under the assumption that $\boldsymbol{\mu}_i(t) = \boldsymbol{\mu}_j(t) = \mu_0[\mathbf{e}_x \cos(\omega_0 t + \delta) + \mathbf{e}_y \sin(\omega_0 t + \delta)]$. Here, δ is some phase difference. A further crucial assumption in the derivation of (23) is that the translational motion of the particles during one rotational period of the field is negligible.

The potential (23) is attractive, which leads to the aforementioned cluster formation. Moreover, in an infinitely extended system, i.e., in the thermodynamic limit, the potential (23) gives rise to a first order phase transition [19].

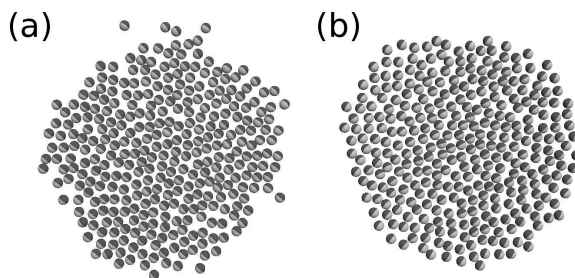


Figure 1. Snapshots of systems at $B_0^* = 50$ and $\omega_0^* = 240$ after clusters have formed. (a) Without and (b) with HIs.

Simulation snapshots of systems after clusters have formed can be seen in figures 1(a) and (b). The former shows the snapshot of a system ($B_0^* = 50$, $\omega_0^* = 240$), whose particles do not interact via HIs, while HIs are included in the system associated with the latter snapshot. Since the formation of clusters can be observed in both the systems, we note as a first result that cluster formation is not prevented by the presence of HIs. As already noted in [19], this is not a priori clear, since HIs can induce additional motion in a nonequilibrium system and the averaged potential (23) is only valid as an approximation to the true interparticle interaction if the translational motion of the particles during one rotational period of the field is small. This is certainly the case for the system without HIs: Inspecting the mean squared displacements (averaged over all the particles) at $B_0^* = 50$ and $\omega_0^* = 240$, we find that the field rotates about 30 times before a particle transverses a distance of its own diameter σ .

The driving frequency $\omega_0^* = 240$ chosen in figure 1 corresponds to $\omega_0 \approx 54$ MHz, if we assume the values of the diffusion constant ($D_0^T \approx 38 \mu\text{m}^2/\text{s}$) and particle size ($\sigma = 13$ nm) that are given in [29] for a ferrofluid.

Note that the cluster formation in infinitely extended quasi-two-dimensional systems corresponds to spinodal decomposition within the coexistence region of a phase transition [19]. This is not exactly true for the cluster formation we observe in the present study. The finite systems considered here do not undergo a phase transition. However, the used system is well suited as a model system to investigate the influence of the HIs on the dynamic behavior of the individual clusters.

In the following we ask how the collective rotational behavior of the particles changes if solvent-mediated interactions are taken into account. First, consider figure 2, which shows whether cluster formation occurs for selected state points in the field strength-frequency domain. Presented are results for both the cases with and without HIs included. Compared to the simple BD system cluster formation breaks down at smaller frequencies ω_0^* in the hydrodynamically interacting system. In the former, cluster formation can be observed up to $\omega_0^* \approx 450$ (at $B_0^* = 50$) while cluster formation ceases at $\omega_0^* \approx 350$ when HIs are present.

To understand the breakdown of cluster formation in more detail, we now examine the rotational motion of the particles. As explained above, synchronized rotation is necessary for (23) to hold, i.e., is a prerequisite for cluster formation. Figure 3 shows the absolute value of the magnetization normalized with respect to its saturation value

$$\frac{M(t)}{M_0} = \frac{1}{N\mu} \left\langle \left| \sum_{i=1}^N \boldsymbol{\mu}_i \right| \right\rangle \quad (24)$$

over the driving frequency ω_0^* of a system [$B_0^* = 50$, cf. Fig. 2] with all the hydrodynamic couplings and without HIs included. The magnetization indicates how aligned the particles are in a given state, i.e., indicates if they follow the field. As can be seen, the magnetization starts with values close to one for both the systems, corresponding to an aligned state. At $\omega_0^* \approx 270$ the magnetization begins to drop for the system that

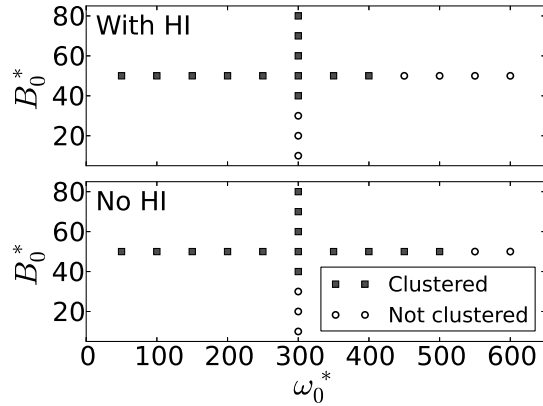


Figure 2. Cluster formation (top) with and (bottom) without HIs in the field strength-frequency domain. Squares/circles indicate where cluster formation occurs/does not occur. The systems are at temperature $T^* = 1$ and dipole moment $\mu^* = 3$.

includes HIs. The magnetization in the system without HIs remains at $M/M_0 \approx 1$ up to $\omega_0^* \approx 420$.

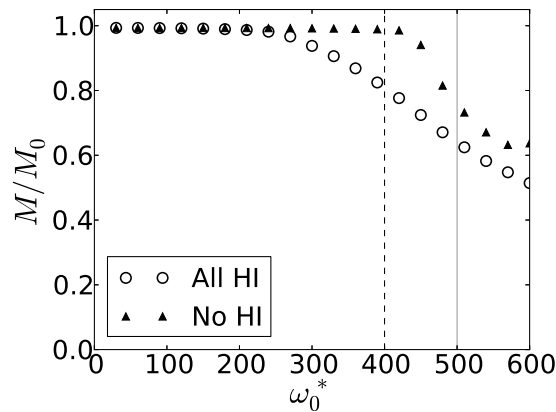


Figure 3. Magnetization normalized with respect to its saturation value over the driving frequency of the external field for a system with and without HIs. The fields used are of strength $B_0^* = 50$. The vertical line indicate where cluster formation ceases with (dashed) and without (solid) HIs.

This magnetization behavior implies that the particles in the hydrodynamically interacting system are less aligned with each other for $\omega_0^* \gtrsim 270$. In particular, the synchronization breaks down at lower frequencies resulting in a premature breakdown of cluster formation.

4. Cluster dynamics

We now turn to the dynamics of the entire cluster. In [19], it was already shown that in systems with HIs, clusters form at a significantly faster pace (as compared to systems without HIs). In this section, we aim to investigate the changes induced by HIs in more detail.

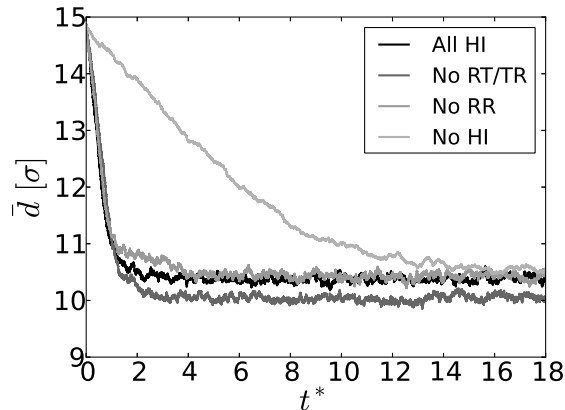


Figure 4. Mean distance between the particles over time \bar{d} in a system ($B_0^* = 50$, $\omega_0^* = 240$) with all hydrodynamic interactions included (All HI), without the hydrodynamic RT/TR coupling (No RT/TR), without the hydrodynamic RR coupling (No RR), and without all HIs (No HI).

First, consider figure 4, which shows the mean distance

$$\bar{d}(t) = \frac{2}{N(N-1)} \sum_{i=1}^N \sum_{j<i} r_{ij}(t) \quad (25)$$

between the particles for a system at $B_0^* = 50$ and $\omega_0^* = 240$. These particular field parameters were chosen for three reasons: First, the frequency is sufficiently high to ensure that the effective potential (23) describes the interparticle interaction well. Second, as seen in figure 2, cluster formation occurs for both a hydrodynamically as well as a not hydrodynamically interacting system. Third, the magnetization of the systems with these choices of ω_0^* and B_0^* is maximal and identical irrespective of the presence of HIs [cf. figure 3].

Specifically, figure 4 shows the evolution of \bar{d} over time for particles interacting via HIs including all the hydrodynamic couplings, for particles lacking the hydrodynamic RT/TR coupling, particles lacking the RR coupling, and particles not interacting via HIs at all. In all the cases, \bar{d} assumes a constant minimal value at long times. To understand this, recall that we consider a single simulation box filled with particles here. In an infinite system, the cluster would keep growing in time indefinitely with a power law behavior [35, 36, 37], since the process corresponds to spinodal decomposition [19]. Here, however, the growth process stops once all the particles have been incorporated into the cluster and a stationary state is reached.

In the systems that include solvent-mediated interactions (All HI, No RT/TR, No RR), the value of \bar{d} drops significantly faster than in the case without any HIs. Consequently, the average distance between the particles decreases faster, which means that the cluster formation process is sped up. The acceleration is neither influenced by the lack of the RT/TR nor the RR coupling, which implies that the TT coupling alone is responsible for this effect. Note, however, that the lack of the presence of the RT/TR coupling expresses itself by a different value of \bar{d} at long times [see figure 4].

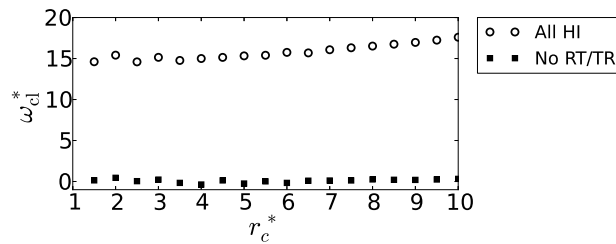


Figure 5. Mean angular frequency ω_{cl}^* around the cluster center of the particles over distance from particle center r_c^* for a system at $B_0^* = 50$ and $\omega_0^* = 240$. Shown are values for a system interacting via all the hydrodynamic couplings and for a system lacking the RT/TR coupling.

The RT/TR coupling does have another interesting influence on the dynamic behavior of the particles. In figure 5, the mean angular frequency of the particles with respect to the cluster center over the distance from the center is shown for a system at $B_0^* = 50$ and $\omega_0^* = 240$. Values for the hydrodynamically interacting case with all the couplings included as well as the case lacking the RT/TR coupling are presented. In the system that includes the RT/TR coupling, the angular velocity of the particles differs from zero at all the displayed distances from the cluster center r_c^* . Hence, the particles perform a rotation around the cluster center in the rotational direction of the external field. The system lacking the RT/TR coupling does not show such a rotational behavior. As can be seen in figure 5, the mean angular frequency of the particle around the cluster center is essentially zero at all distances.

This collective rotation is caused by the individual, field-driven rotations of the particles. The rotational motion of the particles creates a flow field that induces translational motion in all the other particles [see the argument given below (17)-(22)]. Therefore, the TR coupling alone is responsible for this behavior. The RT coupling does not contribute in any way to the cluster rotation.

As we have seen in the previous section, HIs result in a premature breakdown of cluster formation, i.e., a breakdown at smaller driving frequencies of the field (relative to the case without HIs). It stands to reason that the cluster rotation induced by the HIs has a significant influence on this behavior. The particles perform additional translational motion (around the cluster), which makes the effective potential (23) less accurate as a description for the interparticle interaction at a given driving frequency. The more the particles move during one period of the field, the less does the effective

potential capture the actual interaction between the particles.

Finally, note that the RR coupling does not seem to have any significant influence on the dynamic behavior of the cluster. That is, it does not contribute to the accelerated cluster formation or the cluster rotation. The former is illustrated by figure 4, which shows that the mean distance \bar{d} behaves essentially identically to the system with all the HIs included. The fact that the cluster rotation is not influenced by the RR coupling can be seen in figure 5. Despite the presence of the RR coupling, the cluster does not rotate if the RT/TR coupling is absent.

5. Internal structure of the cluster

In a recent experimental study, Weddemann et al. [17] showed the existence of cluster formation in two-dimensional systems of (permanently) dipolar particles that are driven by a rotating external field. In particular, the authors of [17] observed the formation of hexagonally ordered particle agglomerates in their experiments.

The general clustering phenomenon of dipolar particles exposed to rotating fields was later identified as spinodal decomposition in a simulation study by two of the authors of the present study [19]. However, to reproduce clusters of hexagonal order, very low temperatures inside of the two-phase coexistence region had to be considered in computer simulations. It was conjectured that the hexagonally ordered clusters occur in the vapor-solid coexistence region, i.e., at coupling strengths above the ones related to the vapor-liquid region.

As shown in the previous section, HIs can have a significant influence on the collective motion of the particles. Here, in this section, we want to investigate, whether HIs preserve the internal cluster structure. Despite experimental evidence of the hexagonal order, this fact is debatable since it remains unclear to what degree the rotational motion of the magnetic particles in the experimental work [17] follows the dipole moment.

In order to gain insight into the emergent (hexagonal) structures in the present, finite systems, we consider the bond order parameter

$$\psi_6 = \frac{1}{N} \sum_{n=1}^N \frac{1}{|\mathcal{N}_n|} \left| \sum_{k \in \mathcal{N}_n} \exp(i6\pi\phi_{nk}) \right| \quad (26)$$

at different dipolar coupling strengths λ . Here, \mathcal{N}_n is the set of nearest neighbors of particle n , which consists of particles that are closer to particle n than the distance of the first minimum in the pair correlation function of the system. The systems considered in the following are of sufficiently high coupling strength ensuring that cluster formation does indeed occur.

In figure 6, ψ_6 as function of the dipolar coupling strength λ for systems ($B_0^* = 50$) with and without HIs at $\omega_0^* = 240$ and 300 is shown. We note that ψ_6 is essentially independent of time in the stationary situation, where all the particles are part of the cluster. At $\omega_0^* = 300$, the bond order parameter increases with λ for both the

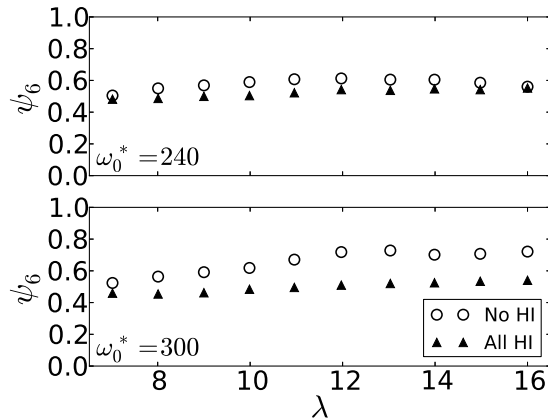


Figure 6. Bond order parameter ψ_6 over coupling strength λ for a system ($B_0^* = 50$, $T^* = 1$) with and without HIs at (top) $\omega_0^* = 240$ and (bottom) $\omega_0^* = 300$.

hydrodynamically as well as the not hydrodynamically interacting system. If HIs are not present, an increase from $\psi_6 \approx 0.52$ at $\lambda = 7.02$ to $\psi_6 \approx 0.72$ at $\lambda = 16$ can be observed. This increase qualitatively agrees with the one observed in the Langevin dynamics simulations in [19]. In the system with HIs included, the bond order parameter ψ_6 increases considerably less with increasing coupling strength. However, there is still significant order in the system.

In the system with $\omega_0^* = 240$ and HIs included, ψ_6 behaves similarly to the case with $\omega_0^* = 300$ and HIs. If these interactions are not taken into account, however, less order than in the $\omega_0^* = 300$ system can be observed. The smaller frequency allows for more translational motion during one rotational period of the field, resulting in more spatial inhomogeneity.

Now consider figure 7, which shows the pair correlation functions of a system ($B_0^* = 50$, $\omega_0^* = 300$) with and without HIs included. The pair correlation function of the not hydrodynamically interacting system shows a double peaked maximum after the first minimum, which is typical for a hexagonally ordered system. The hydrodynamically interacting system, on the other hand, does not have this feature. Hence, the particles tend to have six angularly equally distributed neighbors as shown by the value of ψ_6 [cf. figure 6], but seem to lack the long-range positional order of a hexagonally structured system. Further, the extrema are much more pronounced in the system without HIs, indicating a more ordered state.

In conclusion, in both systems in figure 6, the HIs tend to weaken the hexagonal (or hexatic) order present in the system. The lower value of ψ_6 in systems with HIs can be explained by the collective cluster rotation induced by the hydrodynamic TR coupling. The particles rotate around the cluster center and do not stay at fixed lattice sites. This behavior results in a reduction of the bond order parameter and the hexagonal structure in the system.

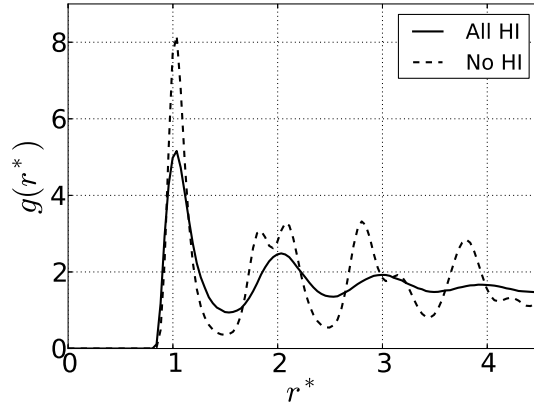


Figure 7. Pair correlation functions of systems at $B_0^* = 50$ and $\omega_0^* = 300$ with and without HIs included.

6. Conclusions

In this study, we have investigated the influence of the solvent on the dynamic behavior of rotationally driven dipolar particles.

The cluster dynamics and formation is influenced in three major ways by HIs. First, HIs accelerate the cluster formation process. While the particle approach each other, flow fields are created that drag other particles along. Second, we have shown HIs to induce a collective cluster rotation. Without HIs no such rotation can be observed. The driven rotating particles pull the solvent with them in their rotational motion, which results in the translational motion of the particles around the cluster center. As a last major point, we have shown cluster formation to cease at lower driving frequencies of the field. We attribute this to an earlier breakdown of synchronization if HIs are present and an increase in translational motion due to the collective cluster rotation.

Moreover, we have studied the influence of HIs on the internal structure of the clusters. Our results indicate that HIs tend to decrease the hexagonal order in the systems.

Recently, one of the authors of this study has conducted an investigation of the structure of a closely related system [38]. The system consisted of particles that only interact via HIs, are confined to a monolayer, and have fixed angular velocities. It was found that hexagonal particle agglomerations rotate, with the hexagonal order melting and recrystallizing periodically. In the system focused on in the present study, no such phenomenon could be observed. We attribute this to the presence of dipolar interactions in our system and a lack of Brownian motion in [38].

Another study has recently investigated the interplay of confinements and HIs [39]. It was shown that particle rotations can be utilized to create directed translational motion in colloids in specific geometries. This result suggests that it might be interesting to examine the effects of different confinements on the dipolar systems considered here.

In conclusion, we have shown that HIs have a considerable influence on the

formation and the dynamics of clusters of driven dipolar colloidal particles in a two-dimensional geometry. Usually, HIs seem to affect colloidal nonequilibrium clustering phenomena less significantly than in the present system. As an example, consider the process of colloidal gelation in two-dimensional Lennard-Jones systems [40]. In contrast to our system, the agglomeration of the particles in [40] is only marginally influenced by the HIs. In general, however, HIs can significantly alter nonequilibrium processes. For instance, HIs can enhance ratchet effects [41, 42] or synchronize the motion of eukaryotic [43] or bacterial [44] flagella.

Acknowledgments

We gratefully acknowledge financial support from the DFG within the research training group RTG 1558 *Nonequilibrium Collective Dynamics in Condensed Matter and Biological Systems*, project B1.

References

- [1] Dzubiella J, Hoffmann G P and Löwen H 2002 *Phys. Rev. E* **65** 021402
- [2] Löwen H 2010 *Soft Matter* **6** 3133
- [3] Kang K, Lettinga M P, Dogic Z and Dhont J K G 2006 *Phys. Rev. E* **74** 026307
- [4] Casic N, Schreiber S, Tierno P, Zimmermann W and Fischer T M 2010 *Europhys. Lett.* **90** 58001
- [5] Wollin C and Stark H 2011 *Eur. Phys. J. E* **34** 42
- [6] Lutz C, Reichert M, Stark H and Bechinger C 2006 *Europhys. Lett.* **74** 719
- [7] Martin J E, Anderson R A and Tigges C P 1998 *J. Chem. Phys.* **108** 3765
- [8] Martin J E, Anderson R A and Tigges C P 1999 *J. Chem. Phys.* **110** 4854
- [9] Martin J E, Venturini E, Odinek J and Anderson R A 2000 *Phys. Rev. E* **61** 2818
- [10] Leunissen M E, Vutukuri H R and Blaaderen A v 2009 *Adv. Mater.* **21** 3116
- [11] Jäger S and Klapp S H L 2011 *Soft Matter* **7** 6606
- [12] Jäger S and Klapp S H L 2011 *Magnetohydrodynamics* **47** 135
- [13] Martin J E, Venturini E, Gulley G and Williamson J 2004 *Phys. Rev. E* **68** 021508
- [14] Osterman N, Poberaj I, Dobnikar J, Frenkel D, Zihlerl P and Babić D 2009 *Phys. Rev. Lett.* **103** 228301
- [15] Douglas J F 2010 *Nature* **463** 302
- [16] Murashov V V and Patey G N 2000 *J. Chem. Phys.* **112** 9828
- [17] Weddemann A, Wittbracht F, Eickenberg B and Hütten A 2010 *Langmuir* **26** 19225
- [18] Wittbracht F, Eickenberg B, Weddemann A and Hütten A 2012 Rotating magnetic field assisted formation of highly ordered two-dimensional magnetic bead arrays *ICQNM 2011, The Fifth International Conference on Quantum, Nano and Micro Technologies* p 99
- [19] Jäger S, Schmidle H and Klapp S H L 2012 *Phys. Rev. E* **86** 011402
- [20] Elsner N, Royall C P, Vincent B and Snoswell D R E 2009 *J. Chem. Phys.* **130** 154901
- [21] Tierno P, Muruganathan R and Fischer T M 2007 *Phys. Rev. Lett.* **98** 028301
- [22] Snoswell D R E, Bower C L, Ivanov P, Cryan M J, Rarity J G and Vincent B 2006 *New Journal of Physics* **8** 267
- [23] Rex M and Löwen H 2008 *Eur. Phys. J. E* **26** 143
- [24] Rinn B, Zahn K and Maret G 1999 *Europhys. Lett.* **46** 537
- [25] Dhont J K G 1996 *An Introduction to Dynamics of Colloids* (Elsevier)
- [26] Reichert M and Stark H 2006 *Phys. Rev. E* **69** 031407
- [27] Allen M P and Tildesley D J 1986 *Computer Simulations of Liquids* (Oxford University Press)

- [28] Ermak D L and McCammon J A 1978 *J. Chem. Phys.* **69** 1352
- [29] Mériguet G, Jardat M and Turq P 2005 *J. Chem. Phys.* **123** 144915
- [30] Dickinson E, Allison S A and McCammon J A 1985 *J. Chem. Soc., Faraday Trans. 2* **81** 591
- [31] Rotne J and Prager S 1969 *J. Chem. Phys.* **50** 4831
- [32] Brańka A C and Heyes D M 1994 *Phys. Rev. E* **50** 4810
- [33] Grandner S and Klapp S H L 2008 *J. Chem. Phys.* **129** 244703
- [34] Halsey T C, Anderson R A and Martin J E 1996 *Int. J. Mod. Phys. B* **10** 3019
- [35] Kabrede H and Hentschke R 2006 *Physica A* **361** 485
- [36] Desai R C and Kapral R 2009 *Dynamics of Self-Organized and Self-Assembled Structures* (Cambridge University Press)
- [37] Majumder S and Das S K 2011 *Europhys. Lett.* **95** 46002
- [38] Stark H *private communication*
- [39] Götze I O and Gompper G 2011 *Phys. Rev. E* **84** 031404
- [40] Yamamoto R, Kim K, Nakayama Y, Miyazaki K and Reichmann D R 2008 *J. Phys. Soc. Jpn.* **77** 084804
- [41] Grimm A and Stark H 2011 *Soft Matter* **7** 3219
- [42] Malgaretti P, Pagonabarraga I and Frenkel D 2012 *ArXiv e-prints (Preprint 1209.4189)*
- [43] Goldstein R E, Polin M and Tuval I 2009 *Phys. Rev. Lett.* **103** 168103
- [44] Reichert M and Stark H 2005 *Eur. Phys. J. E* **17** 493